Available online at www.sciencedirect.com
ScienceDirect
International Journal of Solids and Structures 45 (2008) 3392–3409
INTERNATIONAL JOURNAL OF SOLIDS AND STRUCTURES
www.elsevier.com/locate/ijsolstr

A homogenization-based constitutive model for isotropic viscoplastic porous media

K. Danas [a,b], M.I. Idiart [c], P. Ponte Castañeda [a,b,*]

[a] *Department of Mechanical Engineering and Applied Mechanics, University of Pennsylvania, 220 S. 33rd Street, Philadelphia, PA 19104-6315, USA*
[b] *Laboratoire de Mécanique des Solides, C.N.R.S. UMR7649, Département de Mécanique, École Polytechnique, 91128 Palaiseau Cedex, France*
[c] *Centre for Micromechanics, Cambridge University Engineering Department, Cambridge CB2 1PZ, UK*

Received 14 October 2007; received in revised form 14 January 2008
Available online 15 February 2008

Abstract

An approximate model based on the "second-order" nonlinear homogenization method is proposed to estimate the effective behavior of isotropic, viscoplastic, porous materials. The model is constructed in such a way that it reproduces exactly the behavior of a "composite-sphere assemblage" in the limit of hydrostatic loadings, and therefore coincides with the hydrostatic limit of Gurson's criterion in the special case of ideal plasticity. As a consequence, the new model improves on earlier homogenization estimates, which have been found to be quite accurate for low triaxialities but overly stiff for sufficiently high triaxialities and nonlinearities. Additionally, the estimates delivered by the model exhibit a dependence on the third invariant of the macroscopic stress tensor, which has a nontrivial effect on the effective response of the material at moderate triaxialities. The proposed model is compared with exact results obtained for a special class of porous materials with sequentially laminated microstructures. The agreement is found to be quite good for the entire range of stress triaxialities, and all values of the porosity and nonlinearity considered.

Keywords: Porous media; Homogenization; Viscoplasticity; Constitutive model

1. Introduction

During the last 20 years, several models have been proposed attempting to describe the possible implications of the existence of voids on the overall behavior of metals and other nominally incompressible materials. Perhaps the most popular model for porous plastic solids is that proposed by Gurson (1977), following earlier work by Rice and Tracey (1969). This model makes use of the exact solution for a shell (spherical or

* Corresponding author. Address: Department of Mechanical Engineering and Applied Mechanics, University of Pennsylvania, 220 S. 33rd Street, Philadelphia, PA 19104-6315, USA. Tel.: +1 215 898 5046; fax: +1 215 573 6334.
E-mail addresses: kdanas@seas.upenn.edu (K. Danas), mii23@cam.ac.uk (M.I. Idiart), ponte@seas.upenn.edu (P.P. Castañeda).

0020-7683/$ - see front matter © 2008 Elsevier Ltd. All rights reserved.
doi:10.1016/j.ijsolstr.2008.02.007

cylindrical cavity) under hydrostatic loadings, suitably modified, to obtain estimates for the effective behavior of ideally-plastic solids with isotropic or transversely isotropic distributions of porosity. Several extensions of this model have been proposed over the years, to account for more general constitutive behaviors and porosity distributions. Gologanu et al. (1993, 1997) proposed a refined model for ideally-plastic porous media with more general anisotropic microstructures which, in turn, was generalized to viscoplastic materials by Leblond et al. (1994). Partially inspired by the aforementioned works, Gărăjeu et al. (2000) and Flandi and Leblond (2005a,b) proposed improved models in separate attempts to describe more accurately the evolution of microstructure under axisymmetric loadings. More recently, Monchiet et al. (2007) have proposed a Gurson-type model for ideally-plastic porous media containing prolate and oblate cavities by making use of Eshelby-like trial velocity fields. While these models are exact for the effective behavior of composite-sphere assemblages subjected to purely hydrostatic loadings, they become less accurate at low and moderate triaxial loadings. In addition, they are all derived under the assumption of axisymmetric macroscopic deformations, neglecting any dependence on the third invariant of the macroscopic loading.

In a separate development, Ponte Castañeda (1991) (see also Willis (1991) and Michel and Suquet (1992)) obtained rigorous bounds of the Hashin–Shtrikman type (Hashin and Shtrikman, 1963), as well as estimates of the self-consistent type (Willis, 1977), for porous nonlinear materials by making use—via a suitably designed variational principle—of an optimally chosen "linear comparison composite" (LCC). Generalizing the notion of an optimally selected linear comparison composite to more general types of materials (anisotropic thermoelastic phases), Ponte Castañeda (1996) and Nebozhyn and Ponte Castañeda (1999) proposed improved estimates for two-phase composites, where the effect of the third invariant of the macroscopic stress tensor has been taken into account. However, this so-called "tangent second-order" method can lead to unrealistic predictions for sufficiently strong constitutive nonlinearities (i.e., violation of rigorous bounds, nonconvex effective energy function).

To amend these drawbacks, Ponte Castañeda (2002a) proposed the "second-order" method, which improved on the earlier methods described previously by accounting for the covariance of the local fields in the linear comparison composite, and obtained more accurate estimates for the effective behavior of isotropic porous nonlinear media (Ponte Castañeda, 2002b), when subjected to isochoric loading conditions. However, these estimates have been found to be too "stiff" at sufficiently high triaxialities and nonlinearities (Pastor and Ponte Castañeda, 2002). Following Danas et al. (2008), the present work is focused on improving the estimates delivered by the "second-order" method at high triaxialities, while preserving the high accuracy of the estimates for low triaxialities, as well as the effects of the third invariant of the macroscopic stress tensor on the effective response of the material. Interestingly, it turns out that the dependence of the porous material on the third invariant has important implications on the behavior of the material at high triaxial loadings.

In order to check the accuracy of the new model, the resulting estimates will be compared with exact results for isotropic porous materials with a special class of microstructures known as "sequential laminates" (Ponte Castañeda, 1992; deBotton and Hariton, 2002; Idiart, 2007). As will become clear below, sequential laminates are particularly suitable for assessing the accuracy of "linear comparison" methods like the one considered in this work.

2. Effective behavior

Consider a representative volume element Ω of a two-phase porous medium with each phase occupying a sub-domain $\Omega^{(r)}(r=1,2)$. The vacuous phase is identified with phase 2, whereas the non-vacuous phase (i.e., matrix phase) is denoted as phase 1. The local behavior of the matrix phase is characterized by a convex isotropic stress potential, such that the Cauchy stress $\boldsymbol{\sigma}$ and the Eulerian strain-rate $\boldsymbol{D}$ at any point in $\Omega^{(1)}$ are related by

$$\boldsymbol{D}=\frac{\partial U^{(1)}}{\partial \boldsymbol{\sigma}}(\boldsymbol{\sigma}),\quad U^{(1)}(\boldsymbol{\sigma})=\frac{\dot{\varepsilon}_o\,\sigma_o}{n+1}\left(\frac{\sigma_{\mathrm{eq}}}{\sigma_o}\right)^{n+1}. \tag{1}$$

The von Mises equivalent stress is defined in terms of the deviatoric stress tensor as $\sigma_{\text{eq}} = \sqrt{\frac{3}{2}\boldsymbol{\sigma}' \cdot \boldsymbol{\sigma}'}$, whereas σ_o and $\dot{\varepsilon}_o$ denote the flow stress and reference strain-rate of the matrix phase, respectively. The nonlinearity of the matrix phase is introduced through $m = 1/n$, which denotes the strain-rate sensitivity parameter and takes values between 0 and 1. Note that the two limiting values $m = 1$ and $m = 0$ correspond to linear and ideally-plastic behaviors, respectively.

The effective behavior of the porous material is defined as the relation between the average stress, $\bar{\boldsymbol{\sigma}} = \langle \boldsymbol{\sigma} \rangle$, and the average strain-rate, $\overline{\boldsymbol{D}} = \langle \boldsymbol{D} \rangle$, which can also be characterized by an effective stress potential $\widetilde{U}$, such that (Hill, 1963)

$$\overline{\boldsymbol{D}} = \frac{\partial \widetilde{U}}{\partial \bar{\boldsymbol{\sigma}}}(\bar{\boldsymbol{\sigma}}), \quad \widetilde{U}(\bar{\boldsymbol{\sigma}}) = (1-f) \min_{\boldsymbol{\sigma} \in \mathcal{S}(\bar{\boldsymbol{\sigma}})} \langle U^{(1)}(\boldsymbol{\sigma}) \rangle^{(1)}. \tag{2}$$

The brackets $\langle \cdot \rangle$ and $\langle \cdot \rangle^{(r)}$ denote the volume averages over the representative volume element Ω and over the phases $\Omega^{(r)} (r = 1, 2)$, respectively, f denotes the volume fraction of the porous phase (i.e., the porosity), and $\mathcal{S}(\bar{\boldsymbol{\sigma}}) = \{\boldsymbol{\sigma}, \operatorname{div}\boldsymbol{\sigma} = 0 \text{ in } \Omega,\ \boldsymbol{\sigma}\mathbf{n} = \mathbf{0} \text{ on } \partial\Omega^{(2)},\ \langle \boldsymbol{\sigma} \rangle = \bar{\boldsymbol{\sigma}}\}$ is the set of statically admissible stresses.

In the present work, the focus is on porous materials made up of a random and isotropic distribution of voids in an isotropic matrix phase. It is further noted that overall isotropy implies that, in general, the effective stress potential in relation $(2)_2$ is a function of the three invariants of the stress tensor, $\bar{\boldsymbol{\sigma}}$.

In summary, the problem of estimating the effective behavior of the porous material is equivalent to that of estimating the function $\widetilde{U}$ in relation $(2)_2$. However, computing this function exactly is an extremely difficult task, in general. In the next section, a method for estimating this function is recalled and applied to the class of porous materials of interest in this work. Before proceeding with the analysis, however, it is convenient to introduce the so-called "gauge function."

2.1. The gauge function

From the homogeneity of the local potential $(1)_2$ in $\boldsymbol{\sigma}$, it follows that the effective potential (2) is a homogeneous function of degree $n + 1$ in $\bar{\boldsymbol{\sigma}}$. It is then convenient to introduce the so-called gauge factor Λ, such that (Leblond et al., 1994)

$$\widetilde{U}(\bar{\boldsymbol{\sigma}}) = \frac{\dot{\varepsilon}_o \sigma_o}{n+1} \left(\frac{\Lambda(\bar{\boldsymbol{\sigma}}; f)}{\sigma_o} \right)^{n+1}, \tag{3}$$

which, in turn, allows us to define the gauge function by

$$\widetilde{\Phi}_n(\overline{\boldsymbol{\Sigma}}) = \widetilde{U}(\overline{\boldsymbol{\Sigma}}) - \frac{\dot{\varepsilon}_o \sigma_o^{-n}}{n+1}, \quad \overline{\boldsymbol{\Sigma}} = \frac{\bar{\boldsymbol{\sigma}}}{\Lambda(\bar{\boldsymbol{\sigma}}; f)}, \tag{4}$$

such that the gauge surface is given by $\widetilde{\Phi}_n(\overline{\boldsymbol{\Sigma}}) = 0$. The gauge function is a positively homogeneous function of degree zero in the macroscopic stress $\bar{\boldsymbol{\sigma}}$. Using standard definitions for the stress measures, the normalized macroscopic stress tensor $\overline{\boldsymbol{\Sigma}}$ is written relative to its principal axes as

$$\overline{\boldsymbol{\Sigma}} = \overline{\Sigma}_m \boldsymbol{I} + \overline{\Sigma}_{\text{eq}} \overline{\boldsymbol{S}} = \operatorname{diag}\{\overline{\Sigma}_1, \overline{\Sigma}_2, \overline{\Sigma}_3\}. \tag{5}$$

The stress quantities $\overline{\Sigma}_m = \overline{\Sigma}_{ii}/3$ and $\overline{\Sigma}_{\text{eq}}$ are the normalized macroscopic mean and von Mises equivalent stress, respectively, $\boldsymbol{I}$ is the identity tensor, $\overline{\boldsymbol{S}} = \overline{\boldsymbol{\Sigma}}'/\overline{\Sigma}_{\text{eq}}$ is a normalized stress tensor with $\overline{\boldsymbol{\Sigma}}'$ denoting the stress deviator, while $\overline{\Sigma}_i$ with $i = 1, 2, 3$ denote the three principal values of the normalized macroscopic stress tensor $\overline{\boldsymbol{\Sigma}}$. Making use of the previous notation, it is pertinent to define the following stress invariants

$$X_\Sigma = \frac{\overline{\Sigma}_m}{\overline{\Sigma}_{\text{eq}}}, \quad \cos(3\theta) = \frac{27}{2} \det(\overline{\boldsymbol{S}}). \tag{6}$$

The first is the stress triaxiality, and the second is the Lode angle (Kachanov, 1971) in stress space, which is related to the third invariant of the macroscopic stress tensor. The values $\theta = N\pi/3$ and $\theta = (2N+1)\pi/6$, with N integer, correspond to axisymmetric and simple shear loading conditions, respectively. Relation $(6)_2$

may then be inverted so that, relative to its principal axes, $\overline{\boldsymbol{S}}$ is represented in terms of the Lode angle θ through

$$\overline{\boldsymbol{S}} = \frac{2}{3}\,\mathrm{diag}\Big\{-\cos\Big(\theta+\frac{\pi}{3}\Big), -\cos\Big(\theta-\frac{\pi}{3}\Big), \cos(\theta)\Big\}. \tag{7}$$

Thus, the applied normalized stress tensor $\overline{\boldsymbol{\Sigma}}$ is defined in terms of the three stress invariants, $\overline{\Sigma}_m$, $\overline{\Sigma}_{\mathrm{eq}}$ and θ. Overall isotropy of the material implies then that Φ_n in relation (4) can be expediently written as

$$\widetilde{\Phi}_n(\overline{\boldsymbol{\Sigma}}) = \phi_n(\overline{\Sigma}_1, \overline{\Sigma}_2, \overline{\Sigma}_3) = \widehat{\phi}_n(\overline{\Sigma}_m, \overline{\Sigma}_{\mathrm{eq}}, \theta) = 0, \tag{8}$$

where ϕ_n is a symmetric function of its arguments. At this point, it is also important to mention that as a consequence of definition (1) for the matrix phase, the overall response of the porous material is insensitive to the sign of $\overline{\boldsymbol{\Sigma}}$. This condition may be expressed as $\widetilde{\Phi}_n(\overline{\boldsymbol{\Sigma}}) = \widetilde{\Phi}_n(-\overline{\boldsymbol{\Sigma}})$.

Based now on definition (8), it is convenient to define two cross-sections of the gauge function in order to study in detail the effective response of the porous material. One cross-section of the gauge surface may be defined by considering $\theta = const$. This cross-section lies on a plane which is described by the Cartesian coordinates $\overline{\Sigma}_{\mathrm{eq}}$ and $\overline{\Sigma}_m$, known as the meridional plane. In turn, an alternative cross-section of the gauge function may be considered on a plane defined by a constant hydrostatic pressure, i.e. $\overline{\Sigma}_m = const$. This projection is equivalent to the standard deviatoric $\Pi-$ plane (or octahedral plane) in the theory of plasticity. The polar coordinates on this plane are $r = \sqrt{2/3}\,\overline{\Sigma}_{\mathrm{eq}}$ and the Lode angle θ, respectively. In-plane Cartesian coordinates may also be defined (Lubliner, 1990) by using relations (5) and (7), such that

$$x = \frac{2\overline{\Sigma}_3 - \overline{\Sigma}_1 - \overline{\Sigma}_2}{\sqrt{6}} = \sqrt{\frac{2}{3}}\overline{\Sigma}_{\mathrm{eq}}\cos(\theta) \tag{9}$$

and

$$y = \frac{\overline{\Sigma}_1 - \overline{\Sigma}_2}{\sqrt{2}} = \sqrt{\frac{2}{3}}\overline{\Sigma}_{\mathrm{eq}}\sin(\theta). \tag{10}$$

Similarly, it is useful to introduce the corresponding normalized, macroscopic strain-rate and strain-rate triaxiality measures

$$\overline{\boldsymbol{E}} = \frac{\overline{\boldsymbol{D}}}{\dot{\varepsilon}_o\,(\Lambda(\bar{\boldsymbol{\sigma}}; f)/\sigma_o)^n} = \frac{\partial\Lambda(\bar{\boldsymbol{\sigma}}; f)}{\partial\bar{\boldsymbol{\sigma}}}, \quad X_E = \frac{\overline{E}_m}{\overline{E}_{\mathrm{eq}}}, \tag{11}$$

where the normalized, mean strain-rate is defined as $\overline{E}_m = \overline{E}_{ii}/3$, whereas $\overline{E}_{\mathrm{eq}}$ denotes the von Mises equivalent part of the normalized strain-rate, defined in terms of the deviatoric strain-rate tensor as $\overline{E}_{\mathrm{eq}} = \sqrt{\frac{2}{3}\,\overline{\boldsymbol{E}}' \cdot \overline{\boldsymbol{E}}'}$.

3. Variational estimates

To estimate the effective stress potential $\widetilde{U}$, the "second-order" method, originally proposed by Ponte Castañeda (2002a), is described next. The method is based on the construction of a "*linear comparison composite*" (LCC), with the same microstructure as the nonlinear composite, whose constituent phases are identified with appropriate linearizations of the given nonlinear phases resulting from a suitably designed variational principle. This allows the use of any already available method to estimate the effective behavior of *linear* composites to generate corresponding estimates for *nonlinear* composites.

3.1. Linear comparison composite

For the class of porous materials considered in this work, the corresponding LCC is also a porous material, with a matrix phase characterized by (Ponte Castañeda, 2002a)

$$U_L(\boldsymbol{\sigma}; \check{\boldsymbol{\sigma}}, \mathbf{M}) = U(\check{\boldsymbol{\sigma}}) + \frac{\partial U}{\partial \boldsymbol{\sigma}}(\check{\boldsymbol{\sigma}}) \cdot (\boldsymbol{\sigma} - \check{\boldsymbol{\sigma}}) + \frac{1}{2}(\boldsymbol{\sigma} - \check{\boldsymbol{\sigma}}) \cdot \mathbf{M}(\boldsymbol{\sigma} - \check{\boldsymbol{\sigma}}). \tag{12}$$

The label '1' for the matrix phase will be omitted for simplicity in the rest of the text, except in Section 4. In the last expression, the tensor $\check{\boldsymbol{\sigma}}$ is a uniform, reference stress tensor, which is taken to be *proportional* to the deviatoric macroscopic stress tensor $\bar{\boldsymbol{\sigma}}'$, letting the magnitude of this tensor to be defined later. In turn, $\mathbf{M}$ is a symmetric, fourth-order, compliance tensor, which is initially assumed to be compressible (Ponte Castañeda, 2002a) (the incompressibility limit will be considered later), such that

$$\mathbf{M} = \frac{1}{2\lambda}\,\mathbf{E} + \frac{1}{2\mu}\,\mathbf{F} + \frac{1}{3\kappa}\,\mathbf{J}, \tag{13}$$

with

$$\mathbf{E} = \frac{3}{2}\,\frac{\check{\boldsymbol{\sigma}}' \otimes \check{\boldsymbol{\sigma}}'}{\check{\sigma}_{\mathrm{eq}}^2} = \frac{3}{2}\,\frac{\bar{\boldsymbol{\sigma}}' \otimes \bar{\boldsymbol{\sigma}}'}{\bar{\sigma}_{\mathrm{eq}}^2}, \quad \text{and} \quad \mathbf{F} = \mathbf{K} - \mathbf{E}. \tag{14}$$

In the last two expressions, $\mathbf{K}$ and $\mathbf{J}$ are the standard, fourth-order, isotropic, shear and hydrostatic projection tensors, respectively, while λ and μ are scalars to be defined later. Then, $\mathbf{E}$ and $\mathbf{F}$ correspond to the fourth-order deviatoric eigen-tensors (Ponte Castañeda, 1996) of the tangent compliance tensor, defined as $\mathbf{M}_t = \partial^2 U(\check{\boldsymbol{\sigma}})/(\partial\boldsymbol{\sigma}\partial\boldsymbol{\sigma})$, and are such that $\mathbf{EE} = \mathbf{E}$, $\mathbf{FF} = \mathbf{F}$, $\mathbf{EF} = \mathbf{0}$. Making use of definitions (14), it is easily verified that $\mathbf{E}\,\bar{\boldsymbol{\sigma}} = \bar{\boldsymbol{\sigma}}'$ and $\mathbf{F}\,\bar{\boldsymbol{\sigma}} = \mathbf{0}$. It is also important to note that $\mathbf{E}$ and $\mathbf{F}$ depend explicitly on the Lode angle θ introduced in relation $(6)_2$, and therefore on the third invariant of the macroscopic stress tensor $\bar{\boldsymbol{\sigma}}$.

At this point, it is emphasized that, even though the nonlinear matrix phase is *isotropic* (see relation (1)), the corresponding linearized phase in the LCC is, in general, *anisotropic*. This is in contrast with earlier methods, like the "variational" method introduced by Ponte Castañeda (1991), where the corresponding LCC is locally isotropic. A measure of this anisotropy is given by the ratio

$$k = \lambda/\mu, \tag{15}$$

such that $k = 1$ and $k = 0$ correspond to an isotropic and extremely anisotropic linear matrix phase. Once the linear comparison composite is defined, linear homogenization theories, such as the Hashin–Shtrikman theory (Hashin and Shtrikman, 1963), may be used to estimate the effective behavior of the porous LCC, which in turn can be used, as discussed in the next subsection, to generate corresponding estimates for the nonlinear composite of interest in this work.

Thus, making use of an appropriate specialization of the Levin relations for two-phase thermoelastic materials (Levin, 1967), the effective potential of the LCC can be written as

$$\widetilde{U}_L(\bar{\boldsymbol{\sigma}};\check{\boldsymbol{\sigma}},\mathbf{M}) = (1-f)U(\check{\boldsymbol{\sigma}}) + \boldsymbol{\eta}\cdot(\bar{\boldsymbol{\sigma}} - (1-f)\check{\boldsymbol{\sigma}}) + \frac{1}{2}\,\bar{\boldsymbol{\sigma}}\cdot\widetilde{\mathbf{M}}\,\bar{\boldsymbol{\sigma}} - \frac{1-f}{2}\,\check{\boldsymbol{\sigma}}\cdot\mathbf{M}\check{\boldsymbol{\sigma}}, \tag{16}$$

where $\boldsymbol{\eta} = \partial U/\partial\check{\boldsymbol{\sigma}} - \mathbf{M}\check{\boldsymbol{\sigma}}$, and $\widetilde{\mathbf{M}}$ denotes the effective compliance tensor of the LCC. To estimate $\widetilde{\mathbf{M}}$, use is made of the Willis estimates (Willis, 1977; Ponte Castañeda and Willis, 1995), which are known to be quite accurate for particulate random systems like the ones of interest in this work, up to moderate concentrations of inclusions. For porous materials with isotropic distributions of spherical pores, these estimates take the form

$$\widetilde{\mathbf{M}} = \mathbf{M} + \frac{f}{1-f}\,\mathbf{Q}^{-1}. \tag{17}$$

Here, $\mathbf{Q}$ is a microstructural tensor, related to the Eshelby tensor (Eshelby, 1957), which depends on $\mathbf{M}$ and its inverse $\mathbf{L} = \mathbf{M}^{-1}$, and requires the numerical evaluation of certain integrals. In the special case of statistically isotropic composites, the $\mathbf{Q}$ tensor is given by (Willis, 1977)

$$\mathbf{Q} = \frac{1}{4\pi}\int_{|\zeta|=1} \hat{\mathbf{H}}(\zeta)\,\mathrm{d}S, \quad \hat{\mathbf{H}} = \mathbf{L} - \mathbf{L}\mathbf{H}\mathbf{L}. \tag{18}$$

In this expression, $H_{ijkl} = \left(L_{iakb}\zeta_a\zeta_b\right)^{-1}\zeta_j\zeta_l|_{(ij)(kl)}$, where the brackets denote symmetrization with respect to the corresponding indices. In addition, incompressibility of the nonlinear matrix phase requires the consideration of the incompressibility limit (i.e., $\kappa \to \infty$) in relation $(18)_2$. Nonetheless, the final expression for $\widetilde{\mathbf{M}}$ in relation (17) is compressible, since it corresponds to a porous material. It is also noted that the $\mathbf{Q}$ tensor does not have

the same eigen-tensors as the compliance tensor **M**, and therefore it cannot be written explicitly in terms of **E**, **F** and **J** (Nebozhyn and Ponte Castañeda, 1999). A direct consequence of this fact is that the deformation modes in relation (16) are coupled, as will be seen later. In summary, expressions (16)–(18) completely characterize the LCC in terms of the reference tensor $\check{\boldsymbol{\sigma}}$ and the matrix compliance **M**.

3.2. "Second-order" variational estimate

Once the LCC is defined, the "second-order" estimate for the effective stress potential of the nonlinear porous material is given by (Ponte Castañeda, 2002a; Idiart et al., 2006)

$$\widetilde{U}_{SOM}(\bar{\boldsymbol{\sigma}}) = \operatorname*{stat}_{\lambda,\mu}\{\widetilde{U}_L(\bar{\boldsymbol{\sigma}};\check{\boldsymbol{\sigma}},\mathbf{M}) + (1-f)\,V(\check{\boldsymbol{\sigma}},\mathbf{M})\}, \tag{19}$$

where $\widetilde{U}_L$ is given by (16), and the "corrector" function V is defined as

$$V(\check{\boldsymbol{\sigma}},\mathbf{M}) = \operatorname*{stat}_{\hat{\boldsymbol{\sigma}}}[U(\hat{\boldsymbol{\sigma}}) - U_L(\hat{\boldsymbol{\sigma}};\check{\boldsymbol{\sigma}},\mathbf{M})]. \tag{20}$$

The stationary operation (stat) consists in setting the partial derivative of the argument with respect to the variable equal to zero, which yields a set of nonlinear equations for the variables λ, μ and $\hat{\boldsymbol{\sigma}}$, as shown next.

Making use of the special form (13) of the tensor **M**, we can define two components of the tensor $\hat{\boldsymbol{\sigma}}$ that are 'parallel' and 'perpendicular' to the corresponding reference tensor $\check{\boldsymbol{\sigma}}$, respectively, $\hat{\sigma}_{\parallel} = (\frac{3}{2}\hat{\boldsymbol{\sigma}}\cdot\mathbf{E}\,\hat{\boldsymbol{\sigma}})^{1/2}$ and $\hat{\sigma}_{\perp} = (\frac{3}{2}\hat{\boldsymbol{\sigma}}\cdot\mathbf{F}\,\hat{\boldsymbol{\sigma}})^{1/2}$, such that the equivalent part of the tensor $\hat{\boldsymbol{\sigma}}$ reduces to $\hat{\sigma}_{\rm eq} = \sqrt{\hat{\sigma}_{\parallel}^2 + \hat{\sigma}_{\perp}^2}$. The stationarity operation in (20) then leads to two equations which can be combined into the single equation

$$k\left(\frac{\hat{\sigma}_{\rm eq}}{\check{\sigma}_{\rm eq}}\right)^{1-n} = (k-1)\frac{\hat{\sigma}_{\parallel}}{\check{\sigma}_{\rm eq}} + 1, \tag{21}$$

where k is the ratio defined by (15).

The scalar quantities $\hat{\sigma}_{\parallel}$ and $\hat{\sigma}_{\perp}$ are functions of the applied macroscopic loading $\bar{\boldsymbol{\sigma}}$, the material properties and the microstructure, and result from the stationarity conditions in relation (19) with respect to λ and μ (Ponte Castañeda, 2002a; Idiart et al., 2006):

$$\hat{\sigma}_{\parallel} - \check{\sigma}_{\rm eq} = \sqrt{\frac{3}{1-f}\frac{\partial\widetilde{U}_L}{\partial(2\lambda)^{-1}}} = \sqrt{\frac{3}{1-f}\;\langle(\boldsymbol{\sigma}_L - \check{\boldsymbol{\sigma}})\;\cdot\;\mathbf{E}\,(\boldsymbol{\sigma}_L - \check{\boldsymbol{\sigma}})\rangle^{(1)}} \tag{22}$$

and

$$\hat{\sigma}_{\perp} = \sqrt{\frac{3}{1-f}\frac{\partial\widetilde{U}_L}{\partial(2\mu)^{-1}}} = \sqrt{\frac{3}{1-f}\;\langle\boldsymbol{\sigma}_L\;\cdot\;\mathbf{F}\,\boldsymbol{\sigma}_L\rangle^{(1)}}. \tag{23}$$

The last identities in (22) and (23) are formal and serve to show that the variables $\hat{\sigma}_{\parallel}$ and $\hat{\sigma}_{\perp}$, and thus the linearization scheme, depend on certain traces—given by **E** and **F**—of the fluctuations of the stress field $\boldsymbol{\sigma}_L$ in the LCC. The derivatives $\partial\widetilde{U}_L/\partial(2\lambda)^{-1}$ and $\partial\widetilde{U}_L/\partial(2\mu)^{-1}$ required for the calculation are obtained by differentiation of (16), but are not spelled out here for conciseness. It is noted, however, that they are homogeneous functions of degree zero in **M**, and therefore, the quantities $\hat{\sigma}_{\parallel}$ and $\hat{\sigma}_{\perp}$ depend on the moduli λ and μ only through the anisotropy ratio k. Thus, introducing these expressions for $\hat{\sigma}_{\parallel}$ and $\hat{\sigma}_{\perp}$ into (21), we obtain a single algebraic, nonlinear equation for k, which must be solved numerically for a given choice of the reference tensor $\check{\boldsymbol{\sigma}}$. The evaluation of the two moduli then follows from the relations $\mu = \sigma_o^n/(3\dot{\varepsilon}_o)\,\hat{\sigma}_{\rm eq}^{1-n}$ and $\lambda = k\,\mu$.

Finally, making use of relations (21)–(23), the estimate (19) for the effective stress potential of the nonlinear porous composite can be simplified to

$$\widetilde{U}_{\rm SOM}(\bar{\boldsymbol{\sigma}}) = (1-f)\left[\frac{\dot{\varepsilon}_o\,\sigma_o}{1+n}\left(\frac{\hat{\sigma}_{\rm eq}}{\sigma_o}\right)^{n+1} - \dot{\varepsilon}_o\left(\frac{\check{\sigma}_{\rm eq}}{\sigma_o}\right)^{n}\left(\hat{\sigma}_{\parallel} - \frac{\overline{\sigma}_{\rm eq}}{(1-f)}\right)\right], \tag{24}$$

where the tensor $\check{\boldsymbol{\sigma}}$ remains to be specified.

The corresponding macroscopic stress–strain-rate relation then follows by differentiation of (19) or, equivalently, (24). In the present case, the resulting expression can be shown to reduce to (Idiart and Ponte Castañeda, 2006)

$$\overline{D}_{ij} = (\overline{D}_L)_{ij} + (1-f)\, g_{mn} \frac{\partial \check{\sigma}_{mn}}{\partial \overline{\sigma}_{ij}}, \tag{25}$$

where $\overline{\boldsymbol{D}}_L = \widetilde{\mathbf{M}}\ \bar{\boldsymbol{\sigma}} + \boldsymbol{\eta}$ is the macroscopic strain-rate in the LCC, and the second-order tensor $\boldsymbol{g}$ is given by

$$g_{ij} = \left(\frac{1}{2\lambda} - \frac{1}{2\lambda_t}\right)\left(\hat{\sigma}_{\|} - \frac{\bar{\sigma}_{\mathrm{eq}}}{(1-f)}\right)\frac{\check{\sigma}'_{ij}}{\check{\sigma}_{\mathrm{eq}}} + \frac{f}{2(1-f)^2}\,\bar{\sigma}_{kl}\, T_{klmnij}\, \bar{\sigma}_{mn}, \tag{26}$$

with

$$T_{klmnij} = \left.\frac{\partial [Q(\mathbf{E}(\check{\boldsymbol{\sigma}}))]^{-1}_{klmn}}{\partial \check{\sigma}_{ij}}\right|_{\lambda,\,\mu} \tag{27}$$

and $\lambda_t = \frac{\sigma_o}{3\dot{\varepsilon}_o n}\left(\frac{\check{\sigma}_{\mathrm{eq}}}{\sigma_o}\right)^{1-n}$. It is emphasized that the strain-rate in the nonlinear porous material is not the same as in the LCC. It is also worth noting that in the case of isotropic microstructures considered here, the estimate (25) for $\overline{\boldsymbol{D}}$ is coaxial (i.e., has the same principal directions), but not proportional to, $\bar{\boldsymbol{\sigma}}$. Indeed, the projections of the first term in (25) and the second term in (26) onto the fourth-order tensor $\mathbf{F}$, defined in relation (14), are generally not zero.

3.3. Choices for the reference stress tensor

The estimate (24) requires a prescription for the reference stress tensor $\check{\boldsymbol{\sigma}}$. Physically motivated prescriptions have been proposed by Ponte Castañeda (2002a) and Idiart and Ponte Castañeda (2005). Unfortunately, in the limiting case of hydrostatic loadings, the resulting "second-order" estimates reduce to the earlier "variational" bound of Ponte Castañeda (1991), which is known to be overly "stiff" in that limit. On the other hand, it is precisely in the hydrostatic limit that the effective behavior of 'composite sphere assemblages' (CSAs)—a commonly used model for porous materials—is known exactly and in closed form (Hashin, 1962). Thus, given that a rigorous prescription for $\check{\boldsymbol{\sigma}}$ is yet to be found, an *ad-hoc* prescription is proposed next, in such a way that the resulting "second-order" estimates recover the exact result for CSAs.

To that end, we begin by recalling that the hydrostatic behavior of a CSA can be obtained from the solution of the isolated shell problem, and is characterized by (Leblond et al., 1994)

$$\widetilde{U}_{\mathrm{shell}}(\overline{\sigma}_m) = \frac{\dot{\varepsilon}_o\, \widetilde{\sigma}_H}{1+n}\left(\frac{3}{2}\frac{\overline{\sigma}_m}{\widetilde{\sigma}_H}\right)^{1+n}, \quad \frac{\widetilde{\sigma}_H}{\sigma_o} = \frac{1}{m}(f^{-m}-1), \tag{28}$$

where $\widetilde{\sigma}_H$ is the effective flow stress of the shell, which depends on the porosity f and the strain-rate sensitivity parameter of the matrix $m = 1/n$. On the other hand, the effective flow stress delivered by the "variational" procedure of Ponte Castañeda (1991) (VAR), in the special case of purely hydrostatic loading, reduces to $(28)_1$, with

$$\frac{\widetilde{\sigma}_{H_{\mathrm{VAR}}}}{\sigma_o} = \frac{1-f}{(\sqrt{f})^{1+m}}, \tag{29}$$

which clearly deviates from the exact solution (28) for values of m different from 1 (i.e., the linear case), especially for small porosities.

Recall also that the reference tensor $\check{\boldsymbol{\sigma}}$ has been assumed proportional to $\bar{\boldsymbol{\sigma}}'$, in order to ensure that the effective stress potential $\widetilde{U}_{\mathrm{SOM}}$ is a scalar isotropic function of the macroscopic stress tensor $\bar{\boldsymbol{\sigma}}$. Thus, the following prescription for the reference stress tensor is proposed here:

$$\check{\boldsymbol{\sigma}} = \xi(X_\Sigma, \theta)\bar{\boldsymbol{\sigma}}', \tag{30}$$

where

$$\xi(X_\Sigma,\theta)=\frac{1-tf}{1-f}+\alpha_m(\theta)\ |X_\Sigma|\cdot\left(\exp\left[\frac{-\alpha_{\rm eq}(\theta)}{|X_\Sigma|}\right]+\beta\frac{X_\Sigma^4}{1+X_\Sigma^4}\right) \tag{31}$$

is an empirically chosen interpolating function. In this expression, the coefficients t and β are chosen in an ad-hoc manner to ensure the convexity of the effective stress potential, and are spelled out in Appendix A. On the other hand, the coefficients α_m and $\alpha_{\rm eq}$ are, in general, functions of the microstructure, the nonlinearity m of the matrix, the Lode angle θ, but not of the stress triaxiality X_Σ.

The coefficient α_m is computed such that the estimate for the effective stress potential $\widetilde{U}_{\rm SOM}$, delivered by the "second-order" method in relation (24), coincides with the analytical solution for $\widetilde{U}_{shell}$ in relation (28) in the hydrostatic limit. This condition may be written formally as

$$\widetilde{U}_{\rm SOM}\to\widetilde{U}_{\rm shell}\quad\text{as}\quad|X_\Sigma|\to\infty, \tag{32}$$

which yields a nonlinear algebraic equation for α_m as a function of m, f and θ. In addition to the analytical estimate (28) for the effective stress potential, the solution of the shell problem also requires that the macroscopic deviatoric strain-rate be zero under purely hydrostatic loads. This condition, in turn, provides an equation for the coefficient $\alpha_{\rm eq}$, which can be written as

$$\left(\frac{\partial\widetilde{U}_{\rm SOM}}{\partial\bar{\boldsymbol{\sigma}}}\right)_{\rm eq}\to\left(\frac{\partial\widetilde{U}_{\rm shell}}{\partial\bar{\boldsymbol{\sigma}}}\right)_{\rm eq}\Rightarrow\overline{D}_{\rm eq}\to 0\quad\text{as}\quad|X_\Sigma|\to\infty. \tag{33}$$

While, the computation of the coefficient α_m needs to be performed numerically, the evaluation of $\alpha_{\rm eq}$ can be further simplified to the analytical expression

$$\alpha_{\rm eq}=\alpha_m^{-1}\left[1+\frac{\frac{3}{2}\dot{\varepsilon}_o\left(\check{\sigma}_{\rm eq}/\sigma_o\right)^n-\check{\sigma}_{\rm eq}(2\lambda)^{-1}+\overline{d}_{\|}}{(1-f)\,\hat{\sigma}_{\|}}\left(\frac{1}{2\lambda}-\frac{1}{2\lambda_t}\right)^{-1}\right]. \tag{34}$$

All the quantities involved in the last relation are evaluated in the hydrostatic limit $|X_\Sigma|\to\infty$, while $\overline{d}_{\|}=(3/2)\,\overline{\boldsymbol{S}}\cdot\widetilde{\mathbf{M}}\,\bar{\boldsymbol{\sigma}}$ and λ_t is defined by relation (26). Note that $\alpha_{\rm eq}$ is also a function of m, f and θ.

In summary, relation (30), together with relations (32) and (33) (or (34)), completely define the reference stress tensor $\check{\boldsymbol{\sigma}}$, and thus, the estimate (24) can be used to estimate the effective behavior of the porous material as characterized by relation (24). The strategy followed above was originally put forward by Danas et al. (2008) for transversely isotropic porous media.

At this point, several observations are in order. First, the choice (30) guarantees that the resulting effective stress potential is a homogeneous function of degree $n+1$ in the average stress $\bar{\boldsymbol{\sigma}}$ for all triaxialities $X_\Sigma\in(-\infty,+\infty)$, as it should. Second, it is noted that the choice (30) reduces to

$$\check{\boldsymbol{\sigma}}=\bar{\boldsymbol{\sigma}}', \tag{35}$$

for $X_\Sigma=0$. This is precisely the prescription earlier proposed by Idiart and Ponte Castañeda (2005) (see also Idiart et al. (2006)) for general loadings, which has been found to deliver accurate estimates when the porous composite is subjected to isochoric loadings. Third, because the new prescription (30) is non-zero in the hydrostatic limit, the matrix phase in the LCC remains anisotropic in this limit, in contrast with the earlier choice (35) which leads to an isotropic LCC. This result, together with the fact that the coefficients α_m and $\alpha_{\rm eq}$ depend on the Lode angle θ, implies that the anisotropy ratio k is also a function of θ. Consequently, the effective stress potential $\widetilde{U}_L$ defined in relation (16) depends on θ in the hydrostatic limit. However, it should be emphasized that the predicted effective behavior for hydrostatic loadings is isotropic and depends only on the hydrostatic part of the stress tensor $\overline{\sigma}_m$, the porosity f and the strain-rate sensitivity parameter m. On the other hand, the curvature tensor (Hessian matrix) of the corresponding gauge function in the hydrostatic limit is anisotropic (i.e., it is not proportional to the identity tensor and depends on the Lode angle θ), in contrast to existing methods that do not incorporate any dependence on the third invariant (e.g., the Gurson model).

Ideal plasticity. For the special case of ideal plasticity ($m=0$), relation (28) reduces to

$$\frac{\widetilde{\sigma}_H}{\sigma_o}=\ln\left(\frac{1}{f}\right), \tag{36}$$

and α_m and $\alpha_{\rm eq}$ are determined by relations (32) and (33). On the other hand, the equation describing the effective yield surface, predicted by the "second-order" method, simplifies to

$$\widetilde{\Phi}(\overline{\boldsymbol{\sigma}}) = \hat{\sigma}_{\rm eq} - \sigma_o = \sqrt{\hat{\sigma}_{\parallel}^2 + \hat{\sigma}_{\perp}^2} - \sigma_o = 0, \tag{37}$$

where $\hat{\sigma}_{\parallel}$ and $\hat{\sigma}_{\perp}$ are defined in relations (22) and (23). In the context of these results for the special case of ideally-plastic porous materials, expressions (33) (or (34)) have been assumed to continue to hold for the determination of $\alpha_{\rm eq}$, which implies that the resulting effective yield surface remains smooth for the whole range of stress triaxialities. Further support for this last assumption arises from the fact that—to the best knowledge of the authors—there is no definitive numerical or experimental evidence implying the existence of a vertex in the hydrostatic limit for general isotropic microstructures (but see also Bilger et al. (2005)), in contrast with transversely isotropic microstructures, where the existence of a corner has been observed in yield surfaces obtained by limit analysis procedures (Pastor and Ponte Castañeda, 2002). Note that, for the case of a vertex-like yield surface, the strain-rate $\overline{\boldsymbol{D}}$ would not be uniquely determined at the hydrostatic point.

4. Porous materials with sequentially laminated microstructures

The "second-order" estimate (19) of the previous section involves *two* approximations: the *linearization* of the nonlinear phases (relation (12)) and the *homogenization* of the LCC (relation (16)). For the second approximation, use was made of the Willis estimates (17). These linear estimates are known (Francfort and Murat, 1986; Milton, 2002) to be exact for composites with a special class of "sequentially laminated" microstructures. For this reason, *nonlinear* sequential laminates are particularly appropriate to assess the accuracy of the "second-order" method and, in general, of any LCC-based homogenization method (such as the "variational" method of Ponte Castañeda (1991)), on condition that the Willis estimates be used for the LCC. In this section, exact results for this special class of *nonlinear* sequential laminates are provided.

A sequential laminate is an iterative construction obtained by layering laminated materials (which in turn have been obtained from lower-order lamination procedures) with other laminated materials, or directly with the homogeneous phases that make up the composite, in such a way as to produce hierarchical microstructures of increasing complexity (e.g., Milton, 2002). The *rank* of the laminate refers to the number of layering operations required to reach the final sequential laminate. Of the many possible types of sequential laminates, we restrict attention to porous sequential laminates formed by layering at every step a porous laminate with the matrix phase (denoted as phase 1).

Thus, a rank-1 laminate corresponds to a simple laminate with a given layering direction $\mathbf{n}^{(1)}$, with matrix and porous phases in proportions $1 - f_1$ and f_1. In turn, a rank-2 laminate is constructed by layering the rank-1 laminate with the matrix phase, in a different layering direction $\mathbf{n}^{(2)}$, in proportions f_2 and $1 - f_2$, respectively. Rank-M laminates are obtained by iterating this procedure M times, layering the rank-$(M-1)$ laminate with the matrix phase in the direction $\mathbf{n}^{(M)}$, in proportions f_M and $1 - f_M$, respectively. A key point in this procedure is that the length scale of the *embedded* laminate is assumed to be much smaller than the length scale of the *embedding* laminate. This assumption allows to regard the rank-$(M-1)$ laminate in the rank-M laminate as a homogeneous phase, so that available expressions for the effective potential of simple laminates (e.g., deBotton and Ponte Castañeda, 1992) can be used at each step of the process to obtain an exact expression for the effective potential of the rank-M sequential laminate (e.g., Ponte Castañeda, 1992; deBotton and Hariton, 2002). From this construction process, it follows that the microstructure of these sequential laminates can be regarded as *random* and *particulate*, with phase 1 playing the role of the (continuous) matrix phase embedding the (discontinuous) porous phase. A distinctive feature of this very special class of porous materials is that the strain-rate and stress fields in the *inclusion* phase (in this case, the pores, denoted as phase 2) are uniform.

The effective stress potential of the resulting rank-M porous laminate can be shown to be (deBotton and Hariton, 2002; Idiart, 2006)

$$\widetilde{U}_M(\bar{\boldsymbol{\sigma}}) = \min_{\substack{w_j^{(i)} \\ \bar{\boldsymbol{\sigma}}^{(2)} = 0}} \sum_{i=1}^{M} (1 - f_i) \left(\prod_{j=i+1}^{M} f_j \right) U^{(1)}(\bar{\boldsymbol{\sigma}}_i^{(1)}), \tag{38}$$

where $U^{(1)}$ is the matrix potential given by relation (1), and the stress tensors in the matrix phase, $\bar{\boldsymbol{\sigma}}_i^{(1)}$ $(i = 1, \dots M)$, and the pore phase, $\bar{\boldsymbol{\sigma}}^{(2)}$, are given by

$$\bar{\boldsymbol{\sigma}}_i^{(1)} = \bar{\boldsymbol{\sigma}} + f_i \ \mathbf{w}^{(i)} - \sum_{j=i+1}^{M} (1 - f_j) \ \mathbf{w}^{(j)}, \tag{39}$$

$$\bar{\boldsymbol{\sigma}}^{(2)} = \bar{\boldsymbol{\sigma}} - \sum_{i=1}^{M} (1 - f_i) \ \mathbf{w}^{(i)}. \tag{40}$$

In these expressions, the $\mathbf{w}^{(i)}$, $i = 1, \dots, M$, are second-order tensors of the form

$$\mathbf{w}^{(i)} = w_1^{(i)} \ \mathbf{m}_1^{(i)} \otimes \mathbf{m}_1^{(i)} + w_2^{(i)} \ \mathbf{m}_2^{(i)} \otimes \mathbf{m}_2^{(i)} + w_3^{(i)} \ \mathbf{m}_1^{(i)} \otimes_s \mathbf{m}_2^{(i)}, \tag{41}$$

where $\mathbf{m}_1^{(i)}$ and $\mathbf{m}_2^{(i)}$ are two orthogonal vectors lying on the plane with normal $\mathbf{n}^{(i)}$, and $\otimes_s$ denotes the symmetric part of the outer product. The total porosity f in this rank-M laminate is given in terms of the partial volume fractions f_i by

$$f = \prod_{i=1}^{M} f_i. \tag{42}$$

Thus, expression (38) requires the solution of a $3M$-dimensional convex minimization with respect to the scalar variables $w_\alpha^{(i)}$ $(i = 1, .., M, \ \alpha = 1, 2, 3)$, which, for a given set of f_i and $\mathbf{n}^{(i)}$ and macroscopic stress $\bar{\boldsymbol{\sigma}}$, can be solved numerically using standard numerical techniques. This minimization problem is constrained by the fact that the (uniform) stress in the porous phase $\bar{\boldsymbol{\sigma}}^{(2)}$, as given by (40), must be zero. This constraint (in the variables $w_j^{(i)}$) can be enforced in two different ways. One way is to enforce that the magnitude of the second-order tensor $\bar{\boldsymbol{\sigma}}^{(2)}$ be zero, in which case there is a single *non-linear* constraint, while a different, equivalent way is to enforce that each component of $\bar{\boldsymbol{\sigma}}^{(2)}$ be zero, in which case there are six *linear* constraints (see (40)). The latter approach has been found easier to implement and was therefore adopted in this work.

It is important to note that the effective behavior of the sequential laminates considered here, unlike that of typical nonlinear composites, does not depend on all the details of the microstructure, but only on partial information of it in the form of the volume fractions f_i and lamination directions $\mathbf{n}^{(i)}$. Of particular interest here are porous materials exhibiting overall *isotropic* symmetry. In general, the effective potential (38) will be anisotropic, even if the matrix potential is isotropic. However, appropriate lamination sequences, i.e., particular choices of f_i and $\mathbf{n}^{(i)}$, can be found such that the effective potential (38) tends to be isotropic as the rank M increases (deBotton and Hariton, 2002). To that end, the following lamination sequence has been adopted in this work:

$$f_i = \frac{1 - \frac{i}{M} \ (1 - f)}{1 - \frac{i-1}{M} \ (1 - f)}, \tag{43}$$

and

$$\mathbf{n}^{(i)} = \sin \psi_i \sin \phi_i \ \mathbf{e}_1 + \cos \psi_i \sin \phi_i \ \mathbf{e}_2 + \cos \phi_i \ \mathbf{e}_3, \tag{44}$$

where f is the prescribed porosity in the rank-M laminate, and the angles ψ_i and ϕ_i, which determine the ith direction $(i = 1, \dots, M)$ of lamination relative to a reference basis $\{\mathbf{e}_\alpha\}$, are given by

$$\phi_{j+kM_\eta} = \arccos h_j, \quad h_j = 2\frac{j-1}{M_\eta - 1} - 1, \quad j = 1, \dots, M_\eta, \quad k = 0, \dots, \eta - 1 \tag{45}$$

$$\psi_{j+kM_\eta} = \left(\psi_{j-1} + \frac{3.6}{\sqrt{M_\eta}} \frac{1}{\sqrt{1 - h_j^2}} \right) \bmod 2\pi, \quad j = 2, \dots, M_\eta - 1 \quad \psi_1 = \psi_{M_\eta} = 0. \tag{46}$$

In these expressions, η and M_η are two integers such that the rank of the laminate is $M = \eta M_\eta$. The set of angles (45), (46) corresponds to M_η lamination directions (44), uniformly distributed on the unit sphere (Saff and Kuijlaars, 1997), with η laminations for each direction. It has been verified numerically that, for this specific

lamination sequence, the effective potential (38) becomes progressively less sensitive to the orientation of the principal axes of $\bar{\boldsymbol{\sigma}}$ as the parameters M_η and η increase, meaning that the effective potential tends to be more isotropic with increasing rank. The results provided in the next section correspond to $M = 1500$ with $M_\eta = 50$ and $\eta = 30$.

Finally, the macroscopic strain rate is obtained by differentiating (38) with respect to $\bar{\boldsymbol{\sigma}}$. Noting that the expression is stationary with respect to the variables $w_j^{(i)}$, we have that

$$\overline{\boldsymbol{D}} = \sum_{i=1}^{M}(1-f_i)\left(\prod_{j=i+1}^{M} f_j\right)\frac{\partial U^{(1)}}{\partial \boldsymbol{\sigma}}(\bar{\boldsymbol{\sigma}}_i^{(1)}) + \boldsymbol{\lambda}^{(2)}, \tag{47}$$

where the second-order tensor $\boldsymbol{\lambda}^{(2)}$ is the optimal Lagrange multiplier associated with the traction-free constraint in (38).

5. Results and discussion

This section presents results for the effective behavior and the macroscopic strain-rate fields of isotropic, power-law, porous materials, delivered by the second-order method (SOM), when the choice (30) is made for the reference stress tensor. The predictions of the model proposed in this work are compared with corresponding results generated by the high-rank sequential laminates (LAM) described in Section 4. This comparison is particularly pertinent in view of the fact that power-law, porous, sequential laminates with isotropic microstructures have been found (Idiart, 2007) to reproduce exactly the hydrostatic behavior of the composite-sphere assemblage, as given by (28). For completeness, the SOM estimates are also compared with the earlier "variational" bound (Ponte Castañeda, 1991) (VAR), the Leblond–Perrin–Suquet (LPS) model (Leblond et al., 1994), which reduces to the Gurson model (GUR) (Gurson, 1977) for ideally-plastic media.

Before proceeding with the discussion of the results, it is useful to first introduce the various material and loading parameters used in the plots that follow. The present study is focused on high nonlinearities such as $m = 0.1$ and $m = 0$ (i.e., ideally-plastic materials) and small to moderate porosities, $f = 1, 5, 10\%$. Results for porosity levels below 1%—relevant to ductile fracture—have not been included due to difficulties encountered in the numerical computation of the LAM values. In contrast, it is emphasized that SOM estimates have been obtained for small and dilute porosities and will be reported elsewhere. It is noted, however, that the conclusions drawn below are expected to remain valid at those porosity levels.

As already discussed in a previous section in the context of expression (8), the SOM and the LAM estimates can depend a priori on all three invariants of the macroscopic stress tensor (i.e., on $\overline{\Sigma}_m$, $\overline{\Sigma}_{\rm eq}$ and θ). For completeness, appropriate cross-sections of the gauge surfaces are shown for three representative values of the Lode angle, $\theta = 0, \pi/4, \pi/2$. The value $\theta = 0$ is associated with axisymmetric shear loading. In turn, the value $\theta = \pi/2$ corresponds to simple shear loading, whereas $\theta = \pi/4$ corresponds to a combination of axisymmetric and simple shear loading. It is emphasized that the rest of the models (VAR, LPS and GUR) depend only on the first two invariants, i.e., on $\overline{\Sigma}_m$ and $\overline{\Sigma}_{\rm eq}$.

5.1. Gauge surfaces

Fig. 1 presents various cross-sections of the effective gauge surfaces in the $\overline{\Sigma}_m - \overline{\Sigma}_{\rm eq}$ plane for a fixed nonlinearity $m = 0.1$. In Fig. 1 a the various models are compared for axisymmetric loadings ($\theta = 0$) and a typical porosity $f = 5\%$. The main result in the context of this figure is that the SOM estimates are in very good agreement with the LAM predictions for the entire range of the stress triaxialities ($X_\Sigma \in (-\infty, \infty)$), recovering the exact effective response of a hollow shell subjected to pure hydrostatic loading, as described by relation (28). The fact that the LAM results of Section 4 should agree exactly with the hydrostatic behavior of CSAs in the limit of infinite rank has been shown rigorously by Idiart (2007). Furthermore, the SOM improves "significantly" on the earlier VAR estimate, which in spite of being in good agreement with the LAM results at low triaxialities, it is found to be too stiff at high triaxialities. Indeed, for the given porosity $f = 5\%$, the VAR method predicts that the effective response of the porous material is almost 50% stiffer than the exact shell result of relation (28), when subjected to pure hydrostatic loading. It can be easily verified by comparing

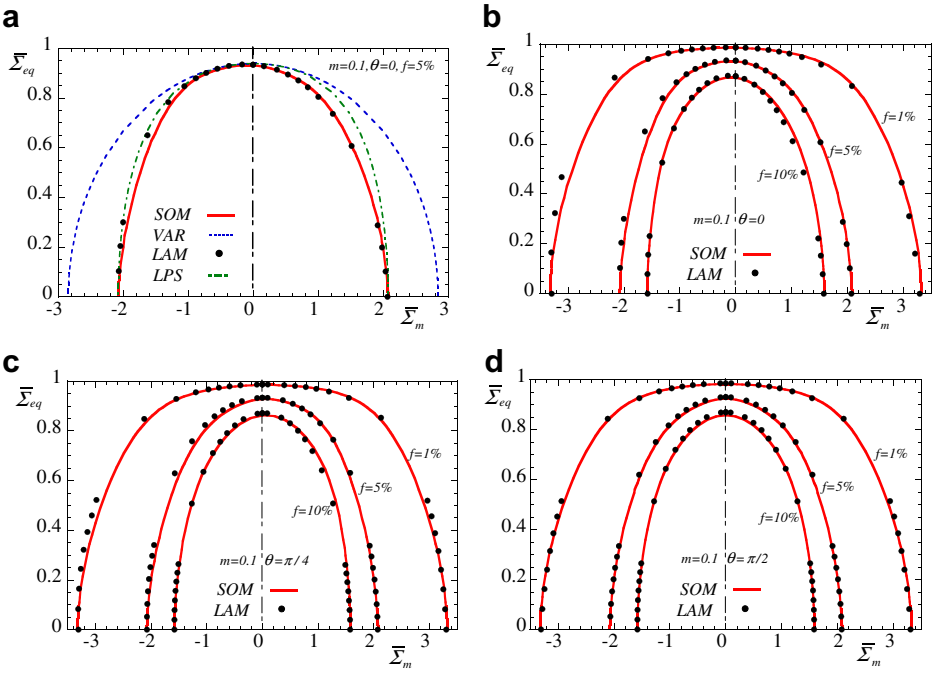

Fig. 1. Gauge surfaces in the $\overline{\Sigma}_{eq} - \overline{\Sigma}_m$ plane; (a) comparison between the various models ("second-order" method SOM, sequential laminates LAM, "variational" bound VAR and Leblond–Perrin–Suquet LPS) for $f = 5\%$ and $\theta = 0$; SOM vs. LAM estimates for (b) $f = 1, 5, 10\%$ and $\theta = 0$; c) $f = 1, 5, 10\%$ and $\theta = \pi/4$; d) $f = 1, 5, 10\%$ and $\theta = \pi/2$.

relations (28) and (29), that the VAR estimate deviates significantly from the analytical shell result for small porosities. On the other hand, the LPS model, even though exact for hydrostatic loading, deviates from the LAM results for moderate to high triaxialities (i.e., approximately $1 \leqslant X_\Sigma \leqslant 10$). On the other hand, the LPS model coincides—by construction—with the VAR bound for isochoric loadings ($X_\Sigma = 0$).

Fig. 1b–d, show cross-sections of the effective gauge surfaces for three different Lode angles, $\theta = 0, \pi/4, \pi/2$, and porosities, $f = 1, 5, 10\%$. In these plots, it is seen that the SOM and the LAM estimates are in very good agreement for the whole range of stress triaxialities, porosities and Lode angles shown. Furthermore, it is interesting to note that for $\theta = 0$ and $\theta = \pi/4$, the gauge curves predicted by both the SOM and the LAM methods are found to be slightly "asymmetric" about the $\overline{\Sigma}_{eq}$-axis, in contrast with the case of $\theta = \pi/2$, where the SOM and the LAM curves are completely symmetric. This "asymmetry" is a direct consequence of the coupling between the three invariants (i.e., $\overline{\Sigma}_m$, $\overline{\Sigma}_{eq}$, θ) in the expression for the gauge function introduced in relation (8). While the SOM and the LAM curves exhibit this particularly interesting behavior, the VAR and the LPS models show a perfect symmetry about the $\overline{\Sigma}_{eq}$-axis. This is a direct consequence of the fact that the VAR and the LPS models involve no dependence on the third invariant of the macroscopic stress tensor, and thus they cannot capture this effect, which, as will be seen later, can become non negligible at high stress triaxialities.

More specifically, for the case of axisymmetric loading ($\theta = 0$) (see Fig. 1b), the SOM and the LAM estimates are found to be slightly stiffer in the negative pressure regime ($\overline{\Sigma}_m < 0$), while the opposite is observed when $\theta = \pi/4$ (see Fig. 1c), i.e., the porous material is stiffer in the positive pressure regime ($\overline{\Sigma}_m > 0$). On the other hand, for $\theta = \pi/2$ (see Fig. 1d), the corresponding gauge curves are completely symmetric about the $\overline{\Sigma}_{eq}$-axis. This can be explained by noting that in the case of $\theta = \pi/2$, the term $\det(\overline{\boldsymbol{\Sigma}}'/\overline{\Sigma}_{eq}) = 0$, which has the implication that the gauge function becomes an even function of the mean macroscopic stress, and therefore is independent of the sign of $\overline{\Sigma}_m$. In contrast, for $\theta = 0$ and $\theta = \pi/4$, the term $\det(\overline{\boldsymbol{\Sigma}}'/\overline{\Sigma}_{eq})$ is not zero and hence the gauge function is not an even function of $\overline{\Sigma}_m$. In addition, it is important to remark that the observed asymmetry of the SOM and the LAM gauge curves about the $\overline{\Sigma}_{eq}$-axis is more pronounced at moderate porosities ($f = 10\%$) than small ones ($f = 1\%$), as can be seen in Fig. 1b–d.

The special case of ideally-plastic porous materials is studied next. Specifically, yield surfaces ($m = 0$) are shown in Fig. 2 for a fixed porosity $f = 5\%$ and $\theta = 0, \pi/2$. Here, the GUR model is also included, whereas LAM estimates are not available for this case due to numerical difficulties. The main observation in the context of this figure is that even though all but the VAR estimate recover the analytical hydrostatic point as discussed in relation (36), the SOM exhibits a softer behavior than the LPS and the GUR models at moderate and high stress triaxialities. In addition, similar to Fig. 1, an interesting effect of the presence of the third invariant is the asymmetry of the yield curve predicted by the SOM about the $\overline{\Sigma}_{eq}$-axis, for the case of $\theta = 0$, as shown in Fig. 2a. In this case, the SOM estimates are found to be slightly stiffer in the negative pressure regime ($\overline{\Sigma}_m < 0$) than in the positive pressure regime ($\overline{\Sigma}_m > 0$). On the contrary, for $\theta = \pi/2$, the corresponding yield curve is symmetric about the $\overline{\Sigma}_{eq}$-axis, since in this case $\det(\overline{\boldsymbol{\Sigma}}'/\overline{\Sigma}_{eq}) = 0$. Furthermore, it is emphasized that the GUR model violates, as already mentioned, the VAR bound at low triaxialities. To amend this drawback of the GUR model at low triaxialities, the LPS model was constructed such that it recovers the VAR bound for isochoric loadings (i.e., $X_\Sigma = 0$), while it lies very close to the GUR model for moderate and high triaxialities.

In summary, the previous analysis, made in the context of Figs. 1 and 2, shows that the effective response of the porous material as predicted by the SOM and the LAM models exhibits somewhat softer behavior when compared with the estimates obtained by the LPS and the GUR models. In addition, the SOM and the LAM estimates depend on the third invariant of the macroscopic stress tensor $\overline{\boldsymbol{\Sigma}}$, in contrast with the rest of the models (VAR, LPS and GUR) which depend only on the first two invariants of $\overline{\boldsymbol{\Sigma}}$. Similar observations have been made in the context of porous, periodic media by Shtern et al. (2002a,b), who introduced the effect of the third invariant of the macroscopic stress tensor in a somewhat ad-hoc manner.

For a better understanding of the effect of the third invariant on the effective response of the porous material, it is useful to show different cross-sections of the gauge surface, as done in Fig. 3 for a fixed porosity $f = 10\%$ and strain-rate sensitivity parameter $m = 0.1$. This cross-section lies on the deviatoric or Π-plane which is defined (see Section 2.1) by considering constant mean stresses, $\overline{\Sigma}_m = 0$ and $\overline{\Sigma}_m = 0.99\overline{\Sigma}_m^H$, with $\overline{\Sigma}_m^H$ denoting the mean stress delivered by the analytical shell result for a given porosity and nonlinearity. The origin of these two graphs corresponds to zero deviatoric macroscopic stress $\overline{\boldsymbol{\Sigma}}'$, while $\overline{\Sigma}_1'$, $\overline{\Sigma}_2'$ and $\overline{\Sigma}_3'$ are the three principal values of $\overline{\boldsymbol{\Sigma}}'$.

Fig. 3a thus presents the deviatoric cross-sections of the gauge functions obtained by the SOM, the LAM and the LPS models for $\overline{\Sigma}_m = 0$. It is recalled that for isochoric loadings, the LPS model is identical to the VAR bound. In this figure, all the methods give very similar predictions for all θ. However, in order to understand further these results, it is useful to recall that overall isotropy of the porous material together with the fact that the corresponding effective gauge function in relation (8) is insensitive to the sign of $\overline{\boldsymbol{\Sigma}}$ (see Section 2.1) yields the continuous and the dotted symmetry lines on the Π-plane (see Fig. 3a). This implies that the whole gauge curve may be constructed by considering stress states in any one of the twelve $(\pi/6)$ segments defined by the continuous and dotted lines, which can be easily verified for all the models shown in Fig. 3a. However, because of the fact that the SOM and the LAM estimates depend slightly on θ in this case of isochoric loadings, the corresponding gauge curves do not form a perfect circular arc at the interval

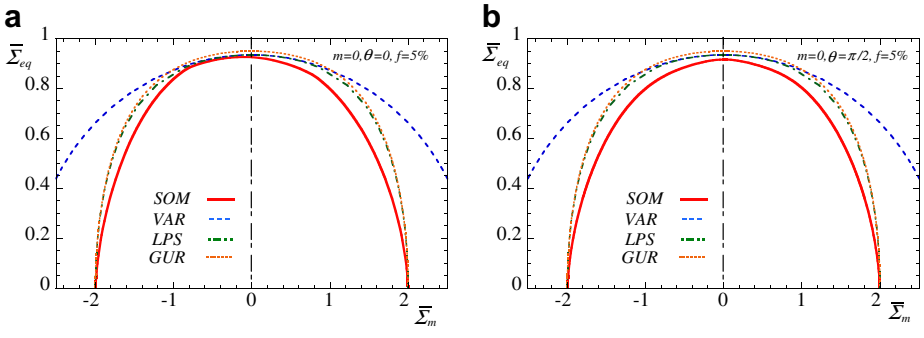

Fig. 2. Yield surfaces for ideally-plastic, porous materials ($m = 0$) for $\theta = 0$ and $\theta = \pi/2$. The Gurson model is also included.

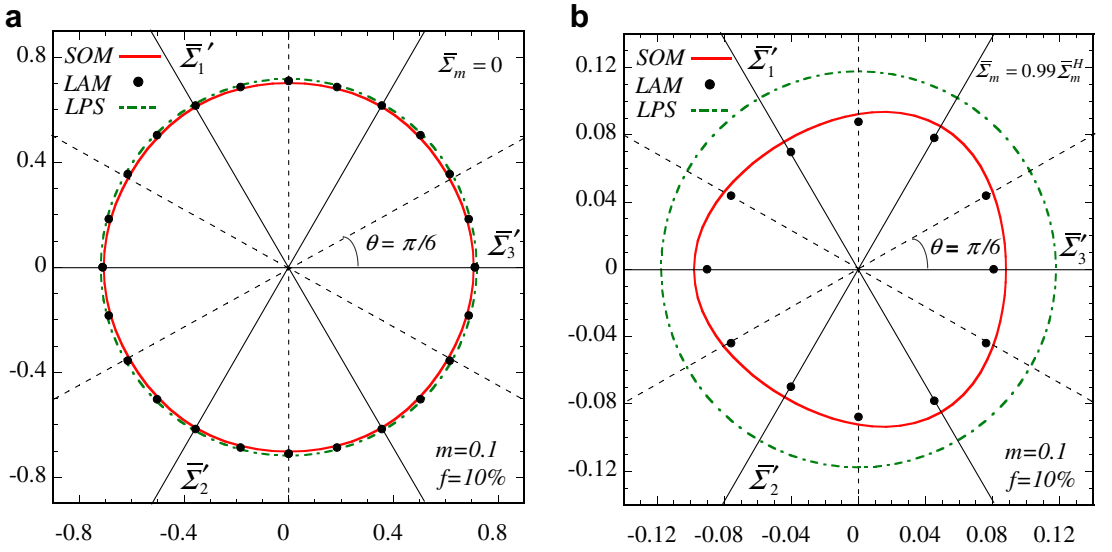

Fig. 3. Cross-sections of gauge functions on the deviatoric plane defined by: (a) a constant pressure $\overline{\Sigma}_m = 0$; (b) a constant pressure $\overline{\Sigma}_m = 0.99\overline{\Sigma}_m^H$, (with $\overline{\Sigma}_m^H$ denoting the mean stress delivered by the analytical shell result).

$0 < \theta < \pi/6$. On the other hand, the LPS (and the VAR) model, which is independent of θ, does form a circle with radius $r = \sqrt{2/3}\,\overline{\Sigma}_{\text{eq}}$.

Considering now the second set of gauge curves in Fig. 3b, it is observed that the shape of the curves delivered by the SOM and the LAM models no longer conform to the above-mentioned $\pi/6$-symmetry. This is because in this case the origin corresponds to zero deviatoric stresses, while the total stress at this point is $\overline{\boldsymbol{\Sigma}} = \overline{\Sigma}_m \boldsymbol{I}$ with $\boldsymbol{I}$ denoting the identity tensor. For this reason, the dotted lines no longer form axes of symmetry, since the corresponding gauge function in relation (8) is insensitive to the sign of $\overline{\boldsymbol{\Sigma}}$ and not the sign of the deviatoric stress $\overline{\boldsymbol{\Sigma}}'$. On the other hand, isotropy of the porous material still requires that the continuous lines form axes of symmetry. This last observation implies that the shape of the gauge curve is determined by each of the "six" $(\pi/3)$ segments formed by the continuous lines. Evidently, all the gauge curves shown in Fig. 3b comply to this requirement. However, as a result of the dependence on the third invariant, the shape of the SOM and LAM cross-sections is substantially different from that of the LPS model which is a perfect circle. The importance of this difference in shape stems from the fact that the normal to the gauge surface prescribes the macroscopic direction of flow.

Before proceeding to the discussion of the corresponding macroscopic strain-rates, it is worth mentioning that McElwain et al. (2006) have recently obtained numerical estimates (using the finite element method) for the effective behavior of *periodic*, ideally-plastic porous media at high porosities ($f > 20\%$). In particular, the resulting yield curves have qualitatively similar shapes to the ones generated by the SOM and the LAM methods in Fig. 3b. These authors have also remarked on the inaccuracy of models making use of only the first two invariants of the macroscopic stress tensor.

5.2. Macroscopic strain rates

For completeness, estimates for the macroscopic equivalent and mean strain-rates, $\overline{E}_{\text{eq}}$ and $\overline{E}_m$, respectively, are presented in this subsection. Thus, Fig. 4 shows estimates for the macroscopic equivalent strain-rate $\overline{E}_{\text{eq}}$ as a function of the porosity and the stress triaxiality X_Σ, for a fixed value of $\theta = 0$ (i.e., axisymmetric loads) and strain-rate sensitivity parameter $m = 0.1$. In particular, Fig. 4a compares the macroscopic equivalent strain-rate estimates obtained by the various models for a porosity, $f = 5\%$. In this case, all the methods are shown to be in good agreement at low stress triaxialities, while they are all somewhat different from the LAM results with increasing stress triaxiality. The SOM estimates are in better agreement with the LAM results in the

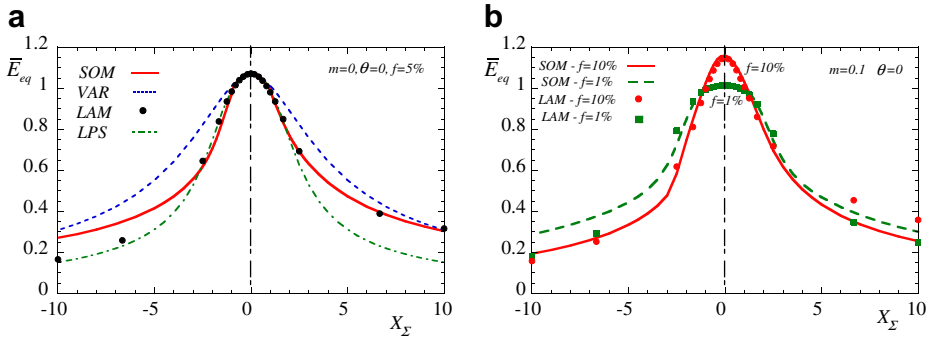

Fig. 4. Plots of the equivalent macroscopic strain-rate $\overline{E}_{\text{eq}}$ as a function of the stress triaxiality X_Σ for $\theta = 0$ and $m = 0.1$; (a) comparison of the various models for a porosity of $f = 5\%$ (b) effect of porosity ($f = 1, 10\%$) on SOM predictions vs. LAM results for $\overline{E}_{\text{eq}}$.

positive triaxiality regime, whereas for negative triaxialities the LPS estimates lie closer to the LAM results, for this particular choice of the porosity and nonlinearity. In turn, the VAR estimates differ significantly from the LAM results at moderate triaxialities. Note that, by definition, all the methods deliver zero equivalent strain-rate in the hydrostatic limit ($|\, X_\Sigma \,| \to \infty$). In turn, in Fig. 4b, the SOM estimates are compared with the LAM estimates for two different porosities, $f = 1,\ 10\%$. In this figure, a clear trend is observed for both the SOM and the LAM curves at low stress triaxialities, where $\overline{E}_{\text{eq}}$ takes higher values at larger porosities, while no such pattern could be observed at higher triaxialities. Nonetheless, the SOM remains in good agreement with the LAM results for the whole range of triaxialities and porosities considered here.

Next, Fig. 5 shows estimates for the mean (hydrostatic) macroscopic strain-rate $\overline{E}_m$ as a function of the porosity and the stress triaxiality X_Σ, for a fixed value of $\theta = 0$ (i.e., axisymmetric loads) and strain-rate sensitivity parameter $m = 0.1$. The SOM and the LAM results are in very good agreement for the whole range of the stress triaxialities and porosities shown here. Particularly, in Fig. 5a, the SOM is found to improve significantly on the earlier "variational" bound VAR, which severely underestimates the macroscopic mean strain-rate at high triaxialities. The LPS model is also in good agreement with the LAM results, although at moderate triaxialities it tends to be slightly stiffer than the SOM estimates. In addition, Fig. 5b shows that the SOM estimates are in excellent agreement with the LAM results for all the porosities considered.

Lastly, it should be emphasized from Figs. 4 and 5 that the equivalent part of the macroscopic strain-rate, $\overline{E}_{\text{eq}}$, is predominant over the corresponding hydrostatic part, $\overline{E}_m$, at low triaxialities, and therefore controls the effective response of the porous material in this regime. For the case of low triaxialities, the SOM is found to be in good agreement with the LAM estimates as discussed in the context of Fig. 4. In turn, the hydrostatic part of the macroscopic strain-rate, $\overline{E}_m$, dominates over the corresponding equivalent part, $\overline{E}_{\text{eq}}$, in the high-triaxiality regime, where the SOM is also found to be in excellent agreement with the LAM, while improving significantly on the earlier VAR estimates. These two observations together suggest that the SOM should be

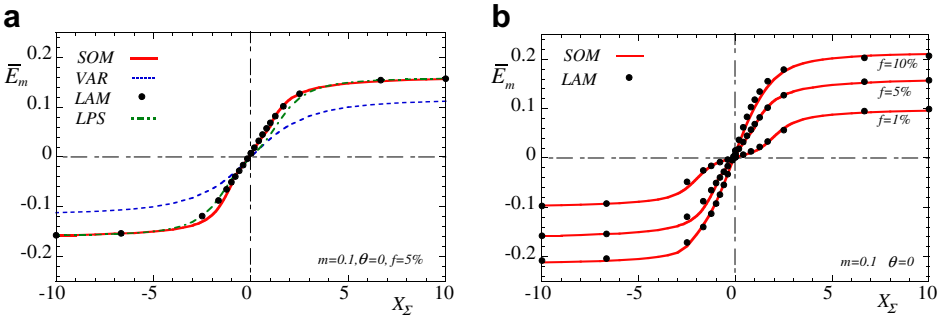

Fig. 5. Plot of the mean macroscopic strain-rate $\overline{E}_m$ as a function of the stress triaxiality X_Σ for $\theta = 0$ and $m = 0.1$; (a) comparison of the various models for a porosity of $f = 5\%$; (b) effect of porosity ($f = 1, 10\%$) on SOM predictions vs. LAM results for $\overline{E}_m$.

able to predict accurately the effective response of the porous material for the entire range of the stress triaxialities, porosities and nonlinearities.

6. Concluding remarks

In this work, a constitutive model for isotropic, porous media has been proposed based on the "second-order" homogenization theory of Ponte Castañeda (2002a). The new model makes use of a novel prescription for the reference stress tensor, given by relation (30), which is such that the resulting "second-order" estimate reproduces exactly the behavior of the "composite-sphere assemblage" in the limit of hydrostatic loading, and therefore coincides with the hydrostatic limit of Gurson's criterion for plastic porous materials.

The new "second-order" model was found to improve significantly on the earlier "variational" estimates of Ponte Castañeda (1991), especially at high stress triaxialities, low porosities and high nonlinearities, where the "variational" bound was known to be overly stiff. Furthermore, the new "second-order" estimates were compared with exact results obtained by high-rank sequential laminates and were found to be in very good agreement for the entire range of stress triaxialities. In comparison, the Leblond et al. (1994) and the Gurson (1977) models were found to be stiffer than the "second-order" estimates for a large range of the stress triaxialities.

In addition, both the "second-order" model and the sequential laminates were found to depend on all the three invariants of the macroscopic stress tensor. Interestingly, the effect of the third invariant was found to be non negligible even at moderate and high triaxialities and moderate porosities leading to an "asymmetric" response of the composite in the Π-plane. On the other hand, the Leblond et al. (1994), the Gurson (1977) and the "variational" model (Ponte Castañeda, 1991) exhibit dependence only on the first two invariants of the macroscopic stress tensor.

It is worth mentioning that even though the interest in this work is on small concentration of the vacuous phase, the above homogenization methods (i.e., "second-order" theory and "variational" bound) may be also applied for composites with high concentration of voids. For example, Despois et al. (2006) have used the "variational" bound to fit experimental data in the context of metal foams. For such high-porosity materials, however, the improvements documented in this work relative to the earlier "variational" model are expected to be comparatively smaller.

As a closing remark, it is emphasized that the new "second-order" model is based on a rigorous variational principle which may be generalized to more complex anisotropic microstructures (arbitrary pore shapes and orientation) and general, three-dimensional loadings, in contrast to the Gurson's model which is restricted to isotropic microstructures, and the Leblond et al. (1994) (Gologanu et al., 1993; Gologanu et al., 1997) method which is valid only for axisymmetric loading conditions (aligned with the pore symmetry axis). The strategy followed in this work can be extended, in principle, to more general constitutive laws (non-power law) for the matrix phase. In fact, the ultimate objective is to develop a *completely general* constitutive model for porous media with evolving anisotropy in the spirit of the earlier works of Ponte Castañeda and Zaidman (1994) and Kailasam and Ponte Castañeda (1998) in the context of the "variational" procedure (Ponte Castañeda, 1991). Such work is in progress (Danas, 2008) and will be reported elsewhere.

Acknowledgements

The work of K.D. was supported by the international fellowship "Gaspard Monge" at the École Polytechnique, and partially by the scholarship for Hellenes of the Alexander S. Onassis Public Benefit Foundation. The work of M.I.I. and P.P.C. was supported by the US National Science Foundation through Grants CMS-02-01454 and OISE-02-31867.

Appendix A. The coefficients of the reference stress tensor

The coefficients introduced in relation (31) are given by

$$t = \frac{1 + X_\Sigma^4}{1 + 2t_1 X_\Sigma^2 + X_\Sigma^4}, \tag{48}$$

with

$$t_1 = 10\left(1 - \left(\frac{\arctan\left(\frac{10^4 f^3}{\exp(-f)}\right)}{\pi/2}\right)^4\right), \tag{49}$$

and

$$\beta = \frac{2}{e}\frac{38m^2}{1+10m^2}\left(1 - \left(\frac{\arctan\left(\frac{10^4 f^2}{\exp(-500f)}\right)}{\pi/2}\right)^6\right). \tag{50}$$

It should be emphasized that the coefficient β becomes approximately zero for porosities larger than 1% and for very high nonlinearities (i.e., m smaller than 0.05) and hence the terms containing β in the definition of the reference stress tensor in relation (31) could be neglected in these cases.

References

Bilger, N., Auslender, F., Bornert, M., Michel, J.-C., Moulinec, H., Suquet, P., Zaoui, A., 2005. Effect of a nonuniform distribution of voids on the plastic response of voided materials: a computational and statistical analysis. Int. J. Solids Struct. 29, 517–538.

Danas, K., 2008. Homogenization-based constitutive model for viscoplastic porous media with evolving microstructure. Ph.D. thesis, University of Pennsylvania.

Danas, K., Idiart, M.I., Ponte Castañeda, P., 2008. A homogenization-based constitutive model for two-dimensional viscoplastic porous media. C.R. Mecanique 336, 79–90.

deBotton, G., Hariton, I., 2002. High-rank nonlinear sequentially laminated composites and their possible tendency towards isotropic behavior. J. Mech. Phys. Solids 50, 2577–2595.

deBotton, G., Ponte Castañeda, P., 1992. On the ductility of laminated materials. Int. J. Solids Struct. 29, 2329–2353.

Despois, J.F., Mueller, R., Mortensen, A., 2006. Uniaxial deformation of microcellular metals. Acta Mater. 54, 4129–4142.

Eshelby, J.D., 1957. The determination of the elastic field of an ellipsoidal inclusion and related problems. Proc. R. Soc. Lond. A 241, 376–396.

Flandi, L., Leblond, J.-B., 2005a. A new model for porous nonlinear viscous solids incorporating void shape effects—I: Theory, Eur. J. Mech. A/Solids 24, 537–551.

Flandi, L., Leblond, J.-B., 2005b. A new model for porous nonlinear viscous solids incorporating void shape effects—I: Numerical validation. Eur. J. Mech. A/Solids 24, 552–571.

Francfort, G., Murat, F., 1986. Homogenization and optimal bounds in linear elasticity. Arch. Rat. Mech. Anal. 94, 307–334.

Gărăjeu, M., Michel, J.-C., Suquet, P., 2000. A micromechanical approach of damage in viscoplastic materials by evolution in size, shape and distribution of voids. Comp. Methods Appl. Mech. Eng. 183, 223–246.

Gologanu, M., Leblond, J.-B., Devaux, J., 1993. Approximate models for ductile metals containing non-spherical voids–case of axisymmetric prolate ellipsoidal cavities. J. Mech. Phys. Solids 41, 1723–1754.

Gologanu, M., Leblond, J.-B., Devaux, J., 1997. Recent extensions of Gurson's model for porous ductile metals. In: Suquet, P. (Ed.), Continuum Micromechanics, . In: CISM Lectures Series. Springer, New York, pp. 1–130.

Gurson, A.L., 1977. Continuum theory of ductile rupture by void nucleation and growth. J. Eng. Mater. Technol. 99, 2–15.

Hashin, Z., 1962. The elastic moduli of heterogeneous materials. J. Appl. Mech., 143–150.

Hashin, Z., Shtrikman, S., 1963. A variational approach to the theory of the elastic behavior of multiphase materials. J. Mech. Phys. Solids 11, 127–140.

Hill, R., 1963. Elastic properties of reinforced solids: some theoretical principles. J. Mech. Phys. Solids 11, 127–140.

Idiart, M.I., 2006. Macroscopic behavior and field statistics in viscoplastic composites. Ph. D. thesis, University of Pennsylvania.

Idiart, M.I., 2007. Nonlinear sequential laminates reproducing hollow sphere assemblages. C.R. Mecanique 335, 363–368.

Idiart, M.I., Danas, K., Ponte Castañeda, P., 2006. Second-order estimates for nonlinear composites and application to isotropic constituents. C.R. Mecanique 334, 575–581.

Idiart, M.I., Ponte Castañeda, P., 2005. Second-order estimates for nonlinear isotropic composites with spherical pores and rigid particles. C.R. Mecanique 333, 147–154.

Idiart, M.I., Ponte Castañeda, P., 2006. Field statistics in nonlinear composites. I: theory. Proc. R. Soc. Lond. A 463, 183–202.

Kachanov, L.M., 1971. Foundations of the Theory of Plasticity. North-Holland, Amsterdam.

Kailasam, M., Ponte Castañeda, P., 1998. A general constitutive theory for linear and nonlinear particulate media with microstructure evolution. J. Mech. Phys. Solids 46, 427–465.

Leblond, J.-B., Perrin, G., Suquet, P., 1994. Exact results and approximate models for porous viscoplastic solids. Int. J. Plasticity 10, 213–235.

Levin, V.M., 1967. Thermal expansion coefficients of heterogeneous materials. Mekh. Tverd. Tela. 2, 8394.

Lubliner, J., 1990. Plasticity Theory. Macmillan Publishing Company.

McElwain, D.L.S., Roberts, A.P., Wilkins, A.H., 2006. Yield criterion for porous materials subjected to complex stress states. Acta Mater. 54, 1995–2002.

Michel, J.C., Suquet, P., 1992. The constitutive law of nonlinear viscous and porous materials. J. Mech. Phys. Solids 40, 783–812.

Milton, G.W., 2002. The Theory of Composites. Cambridge University Press.

Monchiet, V., Charkaluk, E., Kondo, D., 2007. An improvement of Gurson-type models of porous materials by using Eshelby-like trial velocity fields. C.R. Mecanique 335, 32–41.

Nebozhyn, M.V., Ponte Castañeda, P., 1999. The second-order procedure: exact vs approximate results for isotropic, two-phase composites. J. Mech. Phys. Solids 47, 2171–2185.

Pastor, J., Ponte Castañeda, P., 2002. Yield criteria for porous media in plane strain: second-order estimates versus numerical results. C.R. Mecanique 330, 741–747.

Ponte Castañeda, P., 1991. The effective mechanical properties of nonlinear isotropic composites. J. Mech. Phys. Solids 39, 45–71.

Ponte Castañeda, P., 1992. Bounds and estimates for the properties of nonlinear heterogeneous systems. Phil. Trans. R. Soc. Lond. A 340, 531–567.

Ponte Castañeda, P., 1996. Exact second-order estimates for the effective mechanical properties of nonlinear composite materials. J. Mech. Phys. Solids 44, 827–862.

Ponte Castañeda, P., 2002a. Second-order homogenization estimates for nonlinear composites incorporating field fluctuations. I. Theory. J. Mech. Phys. Solids 50, 737–757.

Ponte Castañeda, P., 2002b. Second-order homogenization estimates for nonlinear composites incorporating field fluctuations. II. Applications. J. Mech. Phys. Solids 50, 759–782.

Ponte Castañeda, P., Willis, J.R., 1995. The effect of spatial distribution on the effective behavior of composite materials and cracked media. J. Mech. Phys. Solids 43, 1919–1951.

Ponte Castañeda, P., Zaidman, M., 1994. Constitutive models for porous materials with evolving microstructure. J. Mech. Phys. Solids 42, 1459–1497.

Rice, J.R., Tracey, D.M., 1969. On the ductile enlargement of voids in triaxial fields. J. Mech. Phys. Solids 17, 201–217.

Saff, E.B., Kuijlaars, A.B.J., 1997. Distributing many points on a sphere. The Mathematical Intelligencer 19, 5–11.

Shtern, M.B., Maidanyuk, A.P., Cocks, A., 2002a. ;Effect of the third invariant on the effective reaction of plastic porous bodies. I. Behavior of a porous material unit cell and generalized rule of normality. Powder Metall. Met. C+ 41, 329–335.

Shtern, M.B., Maidanyuk, A.P., Cocks, A., 2002b. Effect of the third invariant on the effective reaction of plastic porous bodies. II. Loading surface of porous bodies whose properties are sensitive to a triaxial stressed state. Powder Metall. Met. C+ 41, 347–354.

Willis, J.R., 1977. Bounds and self-consistent estimates for the overall moduli of anisotropic composites. J. Mech. Phys. Solids 25, 185–202.

Willis, J.R., 1991. On methods for bounding the overall properties of nonlinear composites. J. Mech. Phys. Solids 39, 73–86.